

AIAA-97-2461

## A Review of the Thermal Conductivity of Thin Films

S.R. Mirmira\*, E.E. Marotta\*, and L.S. Fletcher<sup>†</sup>

Conduction Heat Transfer Laboratory  
 Mechanical Engineering Department  
 Texas A&M University  
 College Station, TX

**Abstract**

The thermal conductivity of thin films (0.01-100  $\mu\text{m}$ ) governs the heat transfer characteristics, and hence affects the performance and reliability of microelectronic devices in which they are used. To measure the thermal conductivity of these films, several different techniques (steady state and transient), including the use of laser light have been developed. Further, new methods of thin film deposition have also been developed. This paper reviews these experimental and analytical techniques and the thermal conductivity results obtained. It is shown that the results obtained by these different measurement techniques and deposition methods vary significantly. This emphasizes the importance of measuring the thermal conductivity of thin film materials that closely resemble those being used in the application.

**Nomenclature**

a	radius of film
A	cross sectional area
b	width
C	specific heat
d	diameter of metal line
e	electrical charge
E	exponential function
ef	thermal effusivity
f	frequency
g	ratio of film to substrate effusivity
G	conductance
I	electrical current
k	Boltzmann constant
K	thermal conductivity
l	length of line
L	location of film edge
L <sub>o</sub>	Lorentz constant
N	number of slabs of coating material
q	power output/unit length
R	resistance
t	time
W	width

T	temperature
X	location of sensor
z	layer thickness

**Greek**

$\alpha$	thermal diffusivity
$\beta$	size of microcracks
$\gamma$	fraction cross sectional area covered by microcracks ( $\gamma < 1$ )
$\epsilon$	emissivity
$\lambda$	mean free path of phonons
$\nu$	velocity of sound
$\Delta$	difference
$\rho$	density
$\sigma$	electrical conductivity
$\tau$	time constant
$\omega$	frequency

**Subscripts**

app	apparent
av	average
B	boundary
c	critical
cond	conduction
CR	thermal conduction and radiation
eff	effective
el	electrical contribution
f	film
i	integer
int	internal
la	lattice
m	microcracks
n	net
o	ambient
p	pressure
rad	radiation
s	substrate
slab	slabs of coating material
th	thermal

\*Graduate Research Assistant, Student Member AIAA

<sup>†</sup>Thomas A. Dietz Professor, Fellow AIAA

### Introduction

Knowledge of thermophysical properties, such as thermal conductivity and thermal diffusivity of thin films, is extremely important from the standpoint of heat transport during the nucleation and growth of such films, as well as technological applications of these films. During the use of thin films in devices such as laser diodes and integrated transistor circuits, the heat generated needs to be rapidly dissipated, and hence the thermal conductivity and diffusivity of the film plays an important role. Further, it has been demonstrated that the thermal conductivity of thin films may differ significantly from the bulk values due to microstructural differences and phonon transport between the thin film and the bulk material. Several different techniques have been developed to measure and predict the thermal conductivity of thin film materials. The following section of the paper divides the techniques developed into experimental and analytical, and makes comparisons among them.

### Literature Review

In as much there are a wide range of techniques used to determine the thermal conductivity of thin films, comparisons can only be made in the context of similar techniques. Therefore, this review will categorize the studies in terms of experimental and analytical techniques. The various experimental models are expanded in Table 1, while the analytical models are detailed in Table 2.

### Experimental Techniques

Okuda and Ohkuba<sup>1</sup> developed an experimental technique to measure the thermal conductivity of dielectric films down to a few hundred nanometers in thickness. In this technique a very narrow metal line was produced on the thin film surface by using a photolithography technique. By observing the rate at

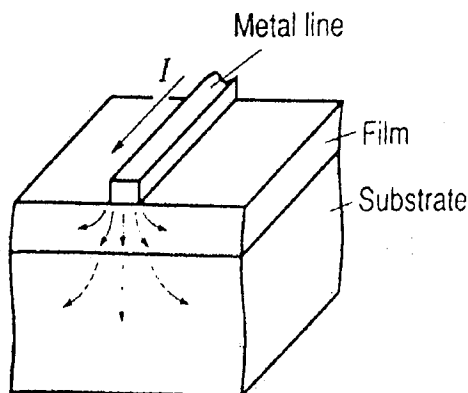


Figure 1. Schematic of experimental geometry.<sup>1</sup>

which the temperature of the metal line increased within a very short period of time (micro-second), it was possible to obtain accurately the thermal conductivity of the substance under the wire line. A schematic of the experimental geometry is shown in Fig. 1. By assuming that the heat capacity of the wire line to be negligible, the temperature change  $\Delta T(t)$  for a line of width  $2d$  was obtained. The change in temperature  $\Delta T(t)$  was determined by measuring the resistance in the line and by calculating  $q$  and  $\tau$  respectively, the thermal conductivity of the film was calculated. Table 1 lists the expression developed by Okuda and Ohkuba.

The success of this technique depends upon the metal line being very narrow, and the transient measurement being conducted with extremely high time resolution. The drawback associated with this technique is that the heat capacity of the metal line cannot be neglected, because very often the thickness of the line is comparable to the film thickness. When the heat capacity of the line is considered, the theory is extremely complex, and has not been completely worked out.

Okuda and Ohkuba used this technique to measure the thermal conductivity of silicon dioxide films 0.1-1  $\mu\text{m}$  in thickness. The thermal conductivity exhibited no significant change over this thickness range. The data are shown in the results section.

Cahill et al<sup>2</sup> reviewed the measuring techniques used for determining the thermophysical properties of thin films. The paper describes three methods, each being used for different film thicknesses.

For film thicknesses of 10  $\mu\text{m}$  and greater, Cahill and Pohl<sup>3</sup> developed an ac (alternating current) technique ( $3\omega$ ) to measure the thermal conductivity and the specific heat. A thin, evaporated metal strip with four pads is used to measure the current and voltage, and is also used as a heater and thermometer, due to the temperature dependent electrical resistance of the metal strip. Figure 2 shows the evaporated metal pattern produced on the face of a sample used for the  $3\omega$  technique. The ac current with an angular frequency of  $\omega$  causes a temperature wave of frequency  $2\omega$  to diffuse into the substrate. The depth of penetration of this wave  $q^{-1}$  and the expression for thermal conductivity are given in Table 1.

The temperature amplitude,  $\Delta T$ , of the heater was found to be inversely proportional to the thermal conductivity of the substrate and to the logarithm of the reciprocal angular frequency. By measuring  $\Delta T$  as a function of  $\omega$ ,  $k$  (thermal conductivity) can be directly determined. In order to measure the thermal conductivity of near surface regions or films on substrates, the angular frequency  $\omega$  is increased. If the

Table 1. Experimental and analytical models for thermal conductivity of thin films.

Investigator	Expressions	Remarks
Experimental Techniques		
Okuda and Ohkuba <sup>1</sup>	$K = -\left(\frac{q}{A(\Delta T / \Delta l)}\right), q = \frac{I^2 R}{l}, \tau = \frac{(\alpha t)^{1/2}}{d}$ $\Delta T = \frac{q}{\pi^{1/2} K} \left[ 1 - \exp\left(\frac{-1}{\tau^2}\right) - \frac{1}{2\pi^{1/2}} \text{Ei}\left(\frac{-1}{\tau^2}\right) \right]$	1. Success depends on metal line being narrow. 2. Extremely high time resolution required. 3. Neglects heat capacity of metal line. 4. Used for SiO <sub>2</sub> thin films.
Cahill et al. <sup>2</sup>	$K = (q^{-1}) \sqrt{2\rho C_p \omega},  q^{-1}  = \left(\frac{\alpha}{2\omega}\right)^{1/2}$	1. 3 $\omega$ technique applicable for film thickness of 10 $\mu\text{m}$ and greater. 2. Insensitive to radiative losses
Cahill et al. <sup>2</sup>	$R_B = \frac{\Delta T}{q / A}$	1. Used for film thickness less than 10 $\mu\text{m}$ . 2. Thermal conductivity is calculated by knowing the thermal boundary resistance.
Zhang and Grigoropoulos <sup>3</sup>	$k = \frac{q}{\Delta T} (L - X)$	1. Free standing thin films. 2. temperature at film edge is assumed to be at room temperature. 3. Used for Si-N films.
Lambropoulos et al. <sup>10</sup>	$\frac{1}{K_{\text{eff}}} = \frac{\pi a}{4 d} \left[ \frac{1}{K_{\text{app}}} - \frac{1}{K_s} \right] \text{---for } d \ll a$ $\frac{1}{K_{\text{app}}} = \frac{1}{K_{\text{eff}}} + \frac{8}{\pi} \frac{1}{K_{\text{eff}}} \sum_{n=1}^{\infty} \theta^n I_n \left( \frac{d}{a} \right) \text{---for } d \approx a$ $\theta = \frac{(K_{\text{eff}} / K_s) - 1}{(K_{\text{eff}} / K_s) + 1}$	1. Apparent thermal conductivity of film/interface assembly is obtained from the calibration curve. 2. Expressions show the explicit dependence of $K_{\text{eff}}$ on $K_{\text{app}}$ and the ratio of $d/a$ . 3. Plot of $d$ versus $K_{\text{eff}}$ yields $K_f^{-1}$
Volklein <sup>11</sup>	$K_f = K_{\text{SiO}_2} d_{\text{SiO}_2} + 2K_{\text{Si}_3\text{N}_4} d_{\text{Si}_3\text{N}_4}$ $\Delta T = \frac{q}{G_{\text{CR}} + G_{\text{RB}}} \left[ 1 - \frac{2}{vb} \tanh\left(\frac{vb}{2}\right) \right]$	1. Steady state. 2. Advantages of sandwich system are its small thickness and high thermal stability, which permits investigation of thin film deposited at high temperatures.
Goodson et al. <sup>16</sup> and Käding et al. <sup>18</sup>	$R_{\text{th}}(d) = \frac{d}{K_{\text{int}}(d)} + R_{\text{B1}} + R_{\text{B2}}$	1. Imperfections in the SiO <sub>2</sub> layer is accounted for in $d/K_{\text{int}}(d)$ 2. Adhesion to and microstructure of the metal is accounted for in $R_{\text{B2}}$ . 3. Incomplete adhesion of oxide is accounted for in $R_{\text{B1}}$ . 4. Not valid for very thin films and at very low temperatures.
Graebner et al. <sup>19,20</sup>	$K = \frac{q}{A(dT/dl)}, A = ZW$ $\frac{K_{\text{rad}}}{K_{\text{cond}}} = \frac{2\epsilon\sigma W^2 T_o^3}{Kd}$	1. The temperature gradient is adjusted to account for radiative losses. 2. The maximum value of the ratio (radiated to conducted heat) was 0.25, implying an error of 25% is radiation is neglected.
Graebner et al. <sup>23</sup>	$K = \rho\alpha C_p$ $\Delta T(t) = (\Delta T)_{\text{max}} \left[ 1 + 2 \sum_{n=1}^{\infty} (-1)^n \exp\left(\frac{-n^2 \pi^2 \alpha t}{d^2}\right) \right]$	1. Method utilizes a high speed laser technique. 2. A non-linear least squares fit of transient temperature response yields, values for $\alpha$ .

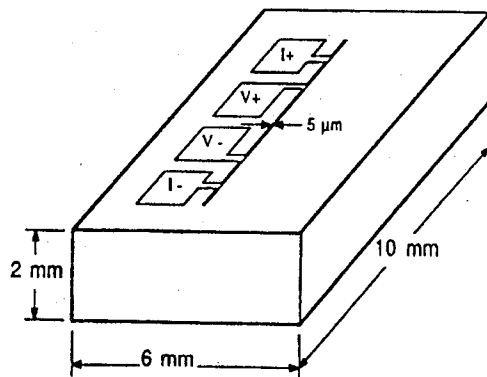


**Figure 2.** Evaporated metal pattern produced on the face of a sample used for the  $3\omega$  technique.<sup>2</sup>

heater/thermometer is evaporated onto a film of thickness  $d$ , on a substrate, the temperature wave will be confined to the film if  $|q^{-1}| < d$ . The measurement of thermal conductivity of thin films on substrates by this technique is highly dependent on the bonding between the film and the substrate.

A technique that enabled the measurement of thermal conductivity of films thinner than 100 Å at the Laboratory of Atomic and Solid State Physics at Cornell University was originally developed by Swartz and Pohl<sup>4</sup> to measure the thermal resistance at the interface of two solids. Figure 3 shows the experimental set up used in this technique. Two metal strips 2 μm apart are vapor deposited onto a dielectric substrate. The electrical resistance of the metal strips is temperature dependent and hence the strips may be used as a thermometers. The interface of interest is the one between the metal strip and the substrate. A large sensing current is induced in one of these metal strips and is used to measure its electrical resistance and hence its temperature. Further, the current causes the temperature of the metal strip to be higher than the that of the substrate. The thermal resistance at the metal strip-substrate interface is given by the expression in Table 1.

The temperature of the dielectric substrate was determined by using the second metal strip as a thermometer, and by inducing a smaller current. The difference in temperature between the second metal strip and the substrate underneath the first metal strip is calculated by integrating the Laplace equation for the geometry shown in Fig 3. Knowing the thermal resistance at the interface, the thermal conductivity of the film may be determined. Cahill et al.<sup>2</sup> claim that this technique may be used to assess the quality of bonding between weakly adhering films to substrates.

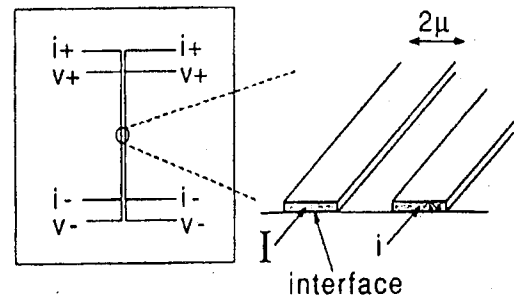


**Figure 3.** Experimental geometry to determine the thermal resistance at solid interfaces.<sup>3</sup>

Lee et al.<sup>5</sup> measured the thermal conductivity of a wide range of oxide thin films deposited via different sputtering techniques using the  $3\omega$  technique. The thermal conductivity of  $\text{SiO}_2$  films deposited via dc and rf magnetron on  $\alpha\text{-SiO}_2$  and  $\text{SiO}_2$  substrates as a function of temperature is shown in the results section. The experimental data obtained indicates a 20% reduction from bulk value and show little dependence on deposition technique or substrate used. For both  $\text{Al}_2\text{O}_3$  and  $\text{SiO}_2$ , the thermal conductivity decreases with a decrease in temperature.

Lee et al. also measured the thermal conductivity of titanium and magnesium oxides ( $\text{TiO}_2$  and  $\text{MgO}$ ). The thermal conductivity of these oxide films is shown as a function of temperature in the results section. The paper concludes that the thermal conductivity of the amorphous oxide thin films ( $\text{Al}_2\text{O}_3$  and  $\text{SiO}_2$ ) were comparable to bulk amorphous oxides, while microcrystalline thin films ( $\text{TiO}_2$ ) may possess thermal conductivity values ranging from low values characteristic of heavily disordered crystals to high thermal conductivities characteristic of bulk materials.

Cahill et al.<sup>6</sup> measured the thermal conductivity of sputtered  $\alpha\text{-Si:H}$  thin films for a hydrogen content of 1-20% and film thickness of 0.2-1.5 μm over a temperature range of 80-400K. A modification of the  $3\omega$  technique was used for this purpose. Five samples of  $\alpha\text{-Si:H}$  of different hydrogen content were deposited on either a  $\text{MgO}$  or  $\text{Si}$  substrate. Although the results indicate that the lowest hydrogen content film does have the highest thermal conductivity, there does not appear to be a strong dependence on hydrogen content. The thermal conductivity as a function of temperature for the sample with a 1% hydrogen content is shown in the results section. The paper also makes a comparison with theoretical results of Feldman et al, who invoked scattering of phonons by tunneling states to produce a finite mean free path

(mfp) for low frequency phonons. Cahill et al. modified this theory by including the contribution of thermal conductivity from vibrational modes of energies less than 10meV. The results obtained by doing so indicate a favorable match between experimental and theoretical values.

Subsequently, Lee and Cahill<sup>7</sup> measured the thermal conductivity of 8-200 nm thick films of SiO<sub>2</sub> and MgO over a temperature range of 78-400 K, by using the  $3\omega$  technique. The apparent thermal conductivity of the thin films was extracted from the finite thermal conductance of the interfaces between the metal film heater and the dielectric layer, and between the dielectric layer and the silicon substrate.

The apparent thermal conductivity values obtained for both SiO<sub>2</sub> and MgO, show a dependence upon temperature. For the plasma enhanced chemical vapor deposited SiO<sub>2</sub>, the apparent thermal conductivity slightly increases with an increase in temperature. A similar trend was observed for the MgO, with a maximum thermal conductivity value being obtained close to room temperature.

In both cases, the apparent thermal conductivity decreases with a decrease in film thickness. Thermal conductivity data for SiO<sub>2</sub> films thicker than 150 nm are only slightly lower than bulk values. These variations in thermal conductivity for SiO<sub>2</sub> and MgO are shown in the results section.

Zhang and Grigoropoulos<sup>8</sup> used a microbridge method to measure the thermal conductivity of a heavily doped free standing polycrystalline silicon film. The experimental set up is shown in Fig 4. A steady state heat flux is generated by passing a dc current in a heater placed at the center of the free standing film. The temperature at the edge of the thin film has been assumed to be room temperature  $T_0$ . The sensor which is a thin metal strip whose resistivity varies with temperature is located at a distance  $X$ . The edge of the free standing thin film is located at a distance  $L$ . The change in voltage across the sensor corresponds to the temperature change of the film at the sensor location. By measuring the heat flux  $q$  at the heater and, and the temperature change  $\Delta T$  at the sensor, the thermal conductivity of the thin film was determined. The expression obtained by Zhang and Grigoropoulos, relating the thermal conductivity is given in Table 1.

The thickness of the thin films were measured by three different techniques: phase shift, amplitude, and the pulse method. The data obtained are shown as a function temperature in the results section. Between 300-400 K, the thermal conductivity remains constant, with the Si-N film 0.6 $\mu$ m in thickness having a slightly higher thermal conductivity value.

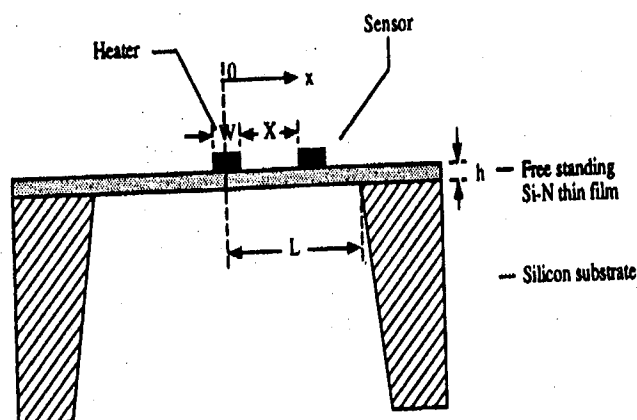
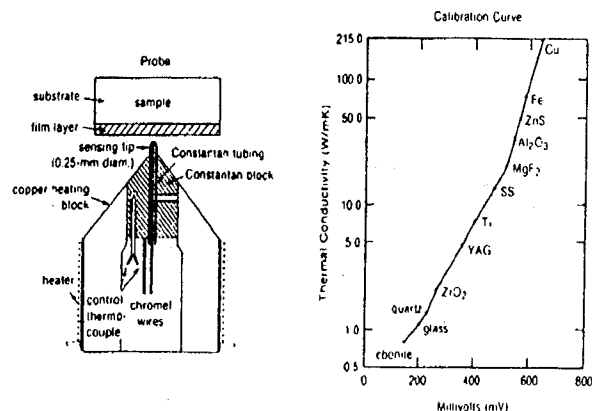


Figure 4. Schematic of a free standing Si-N thin film with a microheater and microsensor.<sup>8</sup>

The thermal comparator technique of measuring thermal conductivity was originally developed for bulk solids. An extensive review has been published by Powell<sup>9</sup>. The procedure involves causing a hot thermocouple junction sensing tip to come in contact with a colder sample surface. A voltage, generated due to the temperature difference between the sensing tip and the reference junction, is recorded by a control module consisting of a personal computer. Several such voltages are recorded, averaged and stored. Thermal conductivity calibration curves are generated for materials of known thermal conductivity, and by comparing materials of unknown thermal conductivity, the thermal conductivity may be determined. Figure 5 shows a schematic of the apparatus for this procedure.

The thermal comparator may also be used to measure the thermal conductivity of thin films applied on substrate materials. Lambropoulos et al<sup>10</sup>. presented an analytical model to determine thin film thermal conductivity using this method knowing the thermal conductivity of the substrate material. The model treats the film/interface/substrate as a semi-infinite body of apparent thermal conductivity  $k_{app}$ , where  $k_{app}$  is directly measured by the thermal comparator. The thin film effective thermal conductivity,  $k_{eff}$ , which includes interfacial effects between the film and the substrate and between the film and the probe tip, is determined using expressions presented in Table 1. In these expressions, 'a' is the film thickness, 't' radius of the film, 't' the film thickness, and  $k_s$  the thermal conductivity of the



**Figure 5.** Principle of operation of a thermal comparator.<sup>10</sup>

substrate material. The thin film thermal conductivity is extracted as the slope of the straight line for the plot of  $t/k_{\text{eff}}$  as a function of film thickness,  $t$ .

The methodology adopted above has the following limitations:

a. If  $k_{\text{app}}$  is close to  $k_s$ , the resolution of the expression for  $K_{\text{eff}}$  becomes poor. For this reason, films which possess thermal conductivities close to that of the substrate may not be accurately tested.

b. The expression for  $K_{\text{eff}}$  is based on the fact that the substrate area is assumed to be a semi-infinite half space. This requires the films to be deposited on large substrates which may be considered as perfect heat sinks.

c. Application of load to ensure good contact between the probe and the film compresses the probe tip into the film/substrate sample and causes localized thinning.

Völklein<sup>11</sup> determined the thermal conductivity of low pressure chemically vapor deposited  $\text{SiO}_2$ - $\text{Si}_3\text{N}_4$  films over a temperature range of 80-400K. A steady state technique utilizing a thin and very small stripe of an electrically conducting material deposited on the film is used for this purpose. The thin stripe known as a bolometer is heated by an alternating current. The authors relate the rise in temperature of the bolometer to the thermal conductivity of the thin films. The measured value of thermal conductivity of the sandwich system at room temperature was 2.4 W/mK. This differs significantly from bulk values of 12W/mK and 17W/mK for  $\text{SiO}_2$  and  $\text{Si}_3\text{N}_4$  respectively. This reiterates the discrepancies that exist between bulk and thin film thermal conductivity values.

Völklein and Kessler<sup>12</sup> used the bolometer technique of developed by Völklein<sup>11</sup> to measure the thermal conductivity of bismuth films ranging from

20-400 nm. As indicated in the results section, the thermal conductivity of the bismuth films decrease with a decrease in thickness. This phenomenon is more pronounced at lower temperatures (100K) where the differences are more significant. If we compare the bulk and thin film thermal conductivity values for bismuth, we notice at lower temperatures the difference are significant, but with an increase in temperature, due to the drastic drop in bulk thermal conductivity, the values are closer. At 400K, the bulk and thin film thermal conductivity values are approximately equal (7W/mK).

Stark et al.<sup>13</sup> utilized the method developed by Völklein<sup>11</sup> as well to determine the thermal conductivity of aluminum oxide films deposited by anodic oxidation. The measurements were made at temperatures ranging from 90-350K. The thermal conductivity ranged from 0.5 W/mK at 90K to approximately 2.0 W/mK at 340K. The trends in thermal conductivity are shown in the results section.

Schafft et al.<sup>14</sup> also studied the thermal conductivity of thin  $\text{SiO}_2$  films. The apparatus used in determining the thermal conductivity were 400 $\mu\text{m}$  long straight line metal structures, or a cross bridge structure. Both structures were equipped with four terminals to permit resistance measurements. The thermal conductivity of thin  $\text{SiO}_2$  films were calculated from the measured joule heating and the temperature drop across the thin film.

The paper reports the thermal conductivity values for two thicknesses (1.74 and 3.04 $\mu\text{m}$ ) of predominantly phosphorous doped silicon dioxide. A comparison with bulk thermal conductivity values indicate that the data obtained for the films is significantly lower. Further, the thermal conductivity decreases with increasing temperature. This trend is opposite to the temperature dependence as reported by Lee and Cahill<sup>7</sup>. The paper suggests that boundary scattering of phonons conducting the heat energy may be the reason for reduced thermal conductivity values, and dependence on thickness of the film.

Brotzen<sup>15</sup> et al. determined the thermal conductivity of silicon dioxide films of four thicknesses deposited by plasma enhanced chemical vapor deposition (PECVD) on monocrystalline silicon substrates. Figure 6 shows a sketch of the test specimen. A constant direct current was passed through the aluminum stripe and the voltage drop was measured. For each current level, the temperature of the aluminum stripe and the silicon heat sink, the current, and voltage were recorded. In order to eliminate directional thermocouple effects, the current direction was reversed after each measurement. By knowing the heat input and the temperature drop, the thermal conductivity of the thin film was determined.

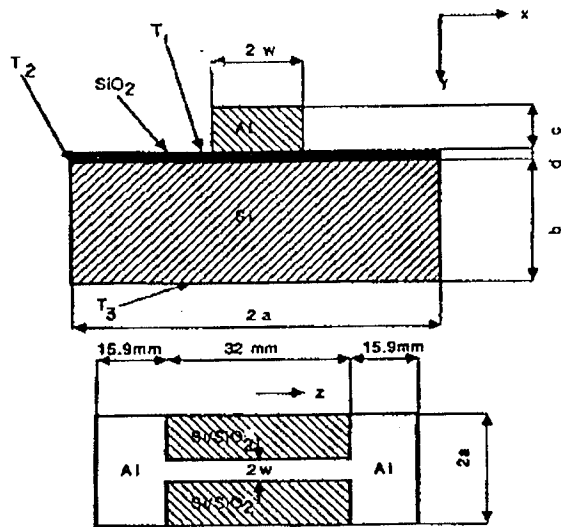


Figure 6. Sketch of test specimen.<sup>15</sup>

The results obtained by Brotzen et al.<sup>15</sup> indicates that the thermal conductivity slightly decreases with increasing temperature. Further, the paper also indicates that different manufacturing/deposition methods create differences in thermal conductivity values. It is evident from the data obtained by Brotzen et al.<sup>15</sup>, that SiO<sub>2</sub> deposited by a two pass PECVD operation possesses a lower thermal conductivity value compared to SiO<sub>2</sub> deposited by a two pass PECVD operation. The paper concludes that the thermal conductivity of SiO<sub>2</sub> films is sensitive to the technique employed in their deposition, since the latter affect the physical and chemical nature of the film.

Goodson et al.<sup>16</sup> studied the annealing temperature dependence of thermal conductivity of low pressure chemical vapor deposited (LPCVD) SiO<sub>2</sub> layers. The paper reports the effective thermal conductivity of undoped LPCVD, thermal, and SIMOX SiO<sub>2</sub> on silicon substrates. The measurement technique utilized was the one developed by Goodson et al.<sup>17</sup>, based on the method of Swartz and Pohl<sup>4</sup>. The data obtained indicates that the effective thermal conductivity for LPCVD SiO<sub>2</sub> increases with thermal processing temperature, at a given layer thickness.

Käding et al.<sup>18</sup> measured the thermal conductivity of thermally grown (TG) and chemical vapor deposited (CVD) silicon dioxide layers 20-200 nm thick by using a non-contact, photothermal technique. Figure 7 shows the experimental geometry for the thermoreflectance measurements. The thermal resistance ( $R_{th}$ ) which is represented by an expression in Table 1, is assumed to consist of an internal volume resistance of the oxide layer ( $d/k_{int}$ ), and boundary resistances between the silicon dioxide and the silicon

( $R_{B1}$ ), and between the silicon dioxide and the metal ( $R_{B2}$ ).

By measuring these thermal resistances, the internal thermal conductivity of the SiO<sub>2</sub> layers was calculated. The data represented in the results section, show a thickness independence and are lower than fused silica values. This may be attributed to the presence of impurities in the silicon dioxide layers.

With the progressive increase in electronic packaging densities, synthetic diamond films are being used as heat spreaders. One of the attractive properties of bulk diamond is its very high thermal conductivity, which in single crystal form can be as high as 2200 W/m<sup>2</sup>K at room temperature. Further, at room temperature, diamond acts as an excellent thermal conductor and electrical insulator. Unfortunately, the thermal conductivity of diamond films may vary by factors of 3 to 5<sup>19</sup> for samples prepared by different techniques.

Graebner et al.<sup>19</sup> developed a technique to measure the thermal conductivity of chemical vapor deposited (CVD) diamond films on silicon. The method involved the deposition of thin film heaters and thermocouples on the surface of the diamond film by standard evaporation techniques using shadow masks. The silicon substrate was etched away completely in a small area, leaving a window of free standing diamond. The dimensions of the window were critical in order to minimize radiative losses. The assets of this technique are that it requires relatively small test specimens, minimized radiation losses, and the deposition technique is not very intricate. The thermal conductivity of the diamond films as a function of film thickness is shown in the results section. The data show a peak at a film thickness of 7.0  $\mu$ m. The range of thermal conductivity values obtained were comparable

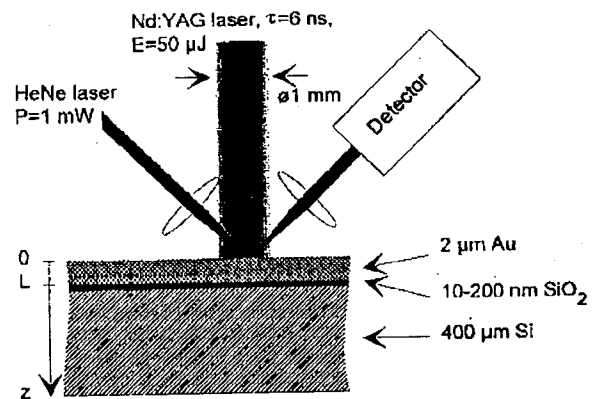


Figure 7. Experimental geometry for thermoreflectance measurements.<sup>18</sup>

to that of copper. Furthermore, compared to diamond in the single crystal form, the data show a decrease by approximately a factor of six.

Graebner et al.<sup>20</sup>, in a subsequent publication reported unusually high thermal conductivity values for diamond films of different thicknesses which were deposited on silicon under similar conditions. The thermal conductivity was measured by a technique described by Berman.<sup>21</sup> The local thermal conductivity values as a function of distance from the bottom are shown in the results section as well. Since the measured thermal conductivity value is an average over the entire thickness of the specimen, the data implies that the local thermal conductivity near the top surface of the 355  $\mu\text{m}$  thick specimen is considerably higher than the measured average value. The paper also reports the variations of thermal conductivity as a function of grain size. The authors attribute the observed gradient in thermal conductivity to the phonon scattering by the roughly cone shaped columnar microstructure.

An important parameter that affects the thermal conductivity of polycrystalline diamond films is its microstructure. Graebner et al.<sup>22</sup> developed a laser technique<sup>23</sup> which enabled them to measure the thermal conductivity of polycrystalline diamond films in a direction perpendicular to the plane of the diamond film. The diamond films were nucleated and grown on commercially available single crystal silicon substrates by microwave enhanced plasma chemical vapor deposition. The average thickness of these films were 28.4, 69.1, 185, and 408  $\mu\text{m}$ . The measured as well the deduced local thermal conductivity data in a direction perpendicular to that of the film are represented in the results section. The authors were able to extract the local thermal conductivity by comparing films of successive thickness. The maximum local thermal conductivity value of 2500 W/mK at 298K is comparable to the value obtained for diamond in the single crystal form. A comparison between the local thermal conductivity in directions parallel and perpendicular to the film shows that the rate at which they increase, with an increase in sample thickness varies. This indicates anisotropy in the local thermal conductivity.

In order to understand these data, we recall that the phonons carrying heat energy are scattered by several mechanisms including: (1) impurities, (2) other high energy phonons, (3) lattice defects, and (4) boundaries. The first three mechanisms contribute approximately twice the amount of resistance attributable to boundary resistance, and the effect of all four mechanisms diminish with an increase in film thickness. This partially explains the decrease in thermal conductivity gradient with an increase in temperature. The anisotropic behavior on the other

hand, is a little more difficult to explain. Transmission electron microscopy (TEM)<sup>24</sup> studies show that lattice imperfections have a tendency to concentrate at grain boundaries, and would probably reflect incident phonons, instead of scattering them isotropically. This would result in a greater decrease of heat transport in the parallel direction as compared to the perpendicular direction.

By assuming that defects are concentrated near grain boundaries, Goodson<sup>25</sup>, related the internal phonon scattering to the local characteristic dimensions in diamond layers. It is evident from the results obtained that the conductivity of layers with larger grains increases far more rapidly with increasing layer thickness. Further, the data show that the thermal conductivity values predicted by Goodson is significantly lower than that for high quality thick CVD diamond layers. This reduction is more predominant at 77K, due to the phonon mean free path being small due to scattering at grain and layer boundaries, as well as the specific heat being lower compared to the value at room temperature. These phenomena cause the thermal conductivity of the diamond layers at 77K to be less than half the value at room temperature.

#### Analytical Models

An empirical relationship for the thermal conductivity of dielectric materials was presented by Ziman<sup>26</sup>. The expression (Table 2) relates the thermal conductivity to the phonon specific heat per unit volume ( $C$ ), the speed of sound ( $v$ ), and the phonon mean free path ( $\lambda$ ). At room temperatures and above,  $\lambda$  varies inversely with temperature, but at low temperatures,  $\lambda$  varies exponentially with temperature. In order to deduce the thermal conductivity from the mean free path, the mean velocity ( $v$ ) is regarded constant. At high temperatures,  $C$  is nearly constant, but as the temperature decreases,  $C$  also decreases, and eventually varies as  $T^3$ , but the exponential variation in  $v$  is dominant, and  $K$  varies exponentially. When the mean free path of the phonons is constant, the thermal conductivity variation reflects the  $T^3$  behavior of the specific heat.

Anderson<sup>27</sup> reported the electrical conductivity of rare earth transition metal (RETM) thin films deposited by vacuum sputtering. The electronic contribution to the thermal conductivity of RETM films was deduced by using the Wiedemann-Franz law. The lattice contribution was estimated to be one third the electronic contribution. The sum of these two components was considered to be the total thermal conductivity value.

The Wiedemann-Franz law is given in Table 2. Kittel<sup>28</sup> argues that the lattice contribution to thermal



**Table 2. Analytical models for thermal conductivity of thin films.**

Analytical Techniques		
Ziman <sup>26</sup>	$K = \frac{1}{3} (Cv\lambda)$	1. Accounts for phonons of all frequencies. 2. Neglects energy dependence of the carrier free paths.
Anderson R.J. <sup>27</sup>	$K_{el} = \sigma L_o T$ , $L_o = \frac{\pi^2}{3} \left( \frac{k}{e} \right)^2$ , $K_{la} = \frac{1}{3} (Cv\lambda)$	1. Wiedemann-Franz law is applicable to only electrically conducting materials. 2. For bulk materials, the lattice component is negligible
Redondo and Beery <sup>29</sup>	$\frac{K_n}{K} = \left[ 1 + \frac{(N_{slab} - 1)(1 - K_m)\beta\gamma}{1 - (1 - K_m)\gamma} \right]$ --- microcrack model  $\frac{K_n}{K} = 1 - (1 - K_c)\gamma$ --- Swiss cheese model	1. Model assumes thin film coatings contain microcracks. 2. Model predicts that imperfections may cause reductions of the order of two or more orders in thermal conductivity. 3. Model suggests a possible mechanism for laser-induced damage of optical coatings.
Swimm <sup>30</sup>	$K = \left( \frac{e^2}{\sqrt{\rho C_p}} \right)$ , $f_c = \left( \frac{\alpha_f}{l_f^2} \right)$ , $g = \frac{e_s}{e_f}$	1. Requires knowledge of bulk material properties. 2. g and f <sub>c</sub> are calculated from phase differences.

conductivity arises due to the heat conduction by quasiparticles and may be expressed as given by Ziman.<sup>27</sup> Table 3 reports the electrical component, lattice contribution, and the total thermal conductivity of four RETM thin films as determined by Anderson. The paper concludes that the thermal conductivity values estimated by this method are one order of magnitude lower than bulk values.

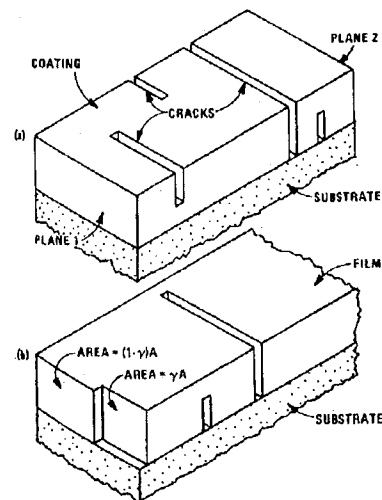
Redondo and Beery<sup>29</sup> developed two models to explain the lower thermal conductivity of thin film materials when compared to the bulk form of the same material. The first model developed by the authors, known as the microcrack model, postulates that the decrease in thermal conductivity is due to the presence of microcracks. It is assumed that these microcracks possess a lower thermal conductivity than the coating. A schematic of the microcrack model is shown in Fig 8. The model predicts the ratio of the net thermal

conductivity to the theoretical thermal conductivity of the film as given by the expression in Table 2. Since the term in brackets is always equal to or greater than unity, we have  $K_{net} \leq K$ . Expressions represented in Table 1 may be used to predict the ratio of thermal conductivities for different values of  $\alpha$ ,  $\beta$ , and  $\gamma$ . It is evident that the net thermal conductivity decreases with a decrease in crack thermal conductivity.

The second model developed by Redondo and Beery accounts for the presence of randomly distributed voids throughout the film. This model was referred to as the Swiss cheese model, and a schematic

**Table 2. Thermal conductivity of RETM thin films.<sup>27</sup>**

Material	$K_{el}$ (W/mK)	$K_{la}$ (W/mK)	$K_{total}$ (W/mK)
Gd <sub>23</sub> Co <sub>77</sub> (planar mag.)	2.8	0.8	3.6
Tb <sub>24</sub> Co <sub>8</sub> Fe <sub>68</sub> (Ion beam)	3.8	1.1	4.9
Tb <sub>21</sub> Co <sub>10</sub> Fe <sub>66</sub> (Triode mag.)	4.9	1.4	6.4
Gd <sub>15</sub> Tb <sub>10</sub> Co <sub>9</sub> Fe <sub>66</sub> (Triode mag.)	3.3	1.0	4.3

**Figure 8. Microcrack and Swiss cheese models.<sup>29</sup>**

representation is also shown in Fig. 8. The ratio of the net thermal conductivity to the theoretical thermal conductivity as predicted by this model is given by the expression in Table 1. In this case as well, the ratio of the thermal conductivity is less than or equal to unity. A comparison of the two models indicates that microcracks can cause reductions of two or more orders of magnitude in the thermal conductivity of the film, whereas, the presence of voids cause only a slight reduction in thermal conductivity.

Swimm<sup>30</sup> published a paper on the photoacoustic determination of thin film thermal properties. This technique allows the individual determination of thermal conductivity and thermal diffusivity, from which the heat capacity per unit volume may be calculated. The thin film measurement is conducted under conditions of: substrate thickness  $\gg$  substrate diffusion length; thin film thickness  $\gg$  thin film optical depth. The author defines the critical frequency  $f_c$ , which is the chopping frequency above which the photoacoustic signal is independent of substrate effects, given in Table 1.

The analysis proceeds by determining the ratio of substrate to film thermal effusivity ( $g$ ) and critical frequency ( $f_c$ ) from the experimental data, and then calculates the thin film thermal conductivity and diffusivity in terms of  $g$ ,  $f_c$ , thin film thickness  $l_f$ , and the known substrate bulk thermal properties of  $k$ ,  $\rho$  and  $C_p$ . Here,  $g$  and  $f_c$  are calculated by measuring the phase differences using the front-surface and rear surface illumination.

### Results

This section of the paper presents the thermal conductivity data for the different materials investigated. Figure 9 shows the data for the thermal conductivity of  $\text{SiO}_2$ ,  $\text{Si:H}$  (1%), and  $\text{Si}_3\text{N}_4$  sandwich system. It is evident from Fig. 9 that  $\text{SiO}_2$  deposited by RF and DC techniques (Lee et al.<sup>5</sup>) have a higher thermal conductivity than that of PECVD  $\text{SiO}_2$  (Lee et al.<sup>7</sup> and Brotzen et al.<sup>15</sup>). Further, the thermal conductivity of phosphorus based  $\text{SiO}_2$  (Schafft et al.<sup>14</sup>) is comparable to data for PECVD  $\text{SiO}_2$ . All these data are slightly lower than the bulk  $\text{SiO}_2$  value. On the other hand,  $\text{Si:H}$  (1%) and the  $\text{Si}_3\text{N}_4$  sandwich system, possess a thermal conductivity higher than the bulk value.

Figure 10 shows the thermal conductivity of  $\text{SiO}_2$  as a function of thickness of the film. The data obtained by Okuda and Ohkuda<sup>1</sup> are comparable to those for bulk thermal conductivity values. Furthermore, it is evident that CVD  $\text{SiO}_2$  appears to possess a slightly lower thermal conductivity value than the TG  $\text{SiO}_2$  specimens (Kading et al.<sup>18</sup>). Figure 10 also shows that the thermal conductivity data for

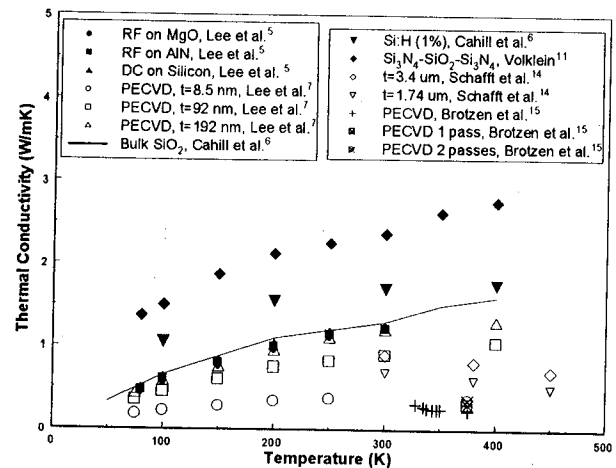


Figure 9. Thermal conductivity of  $\text{SiO}_2$ ,  $\text{Si:H}$  (1%), and  $\text{Si}_3\text{N}_4$  sandwich system as a function of temperature.

thermal and SIMOX samples (Goodson et al.<sup>16</sup>) are extremely close to the bulk  $\text{SiO}_2$  value. This is contradictory to all the existing data for  $\text{SiO}_2$  layers manufactured using other techniques. The difference in results reported by Goodson et al.<sup>16</sup> and Lambropoulos et al.<sup>10</sup> is possibly due to the difference in deposition techniques (LPCVD versus ion and electron beam sputtering). A comparison of data obtained by Goodson et al.<sup>16</sup> and Brotzen et al.<sup>15</sup> (PECVD  $\text{SiO}_2$ ) clearly indicates that the fabrication process strongly influences the thermal conductivity of  $\text{SiO}_2$  thin films.

Figure 11 indicates the thermal conductivity data for several different thin film materials. It is evident

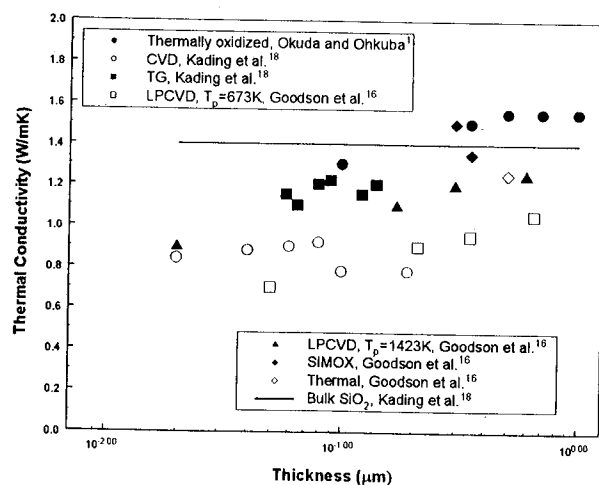
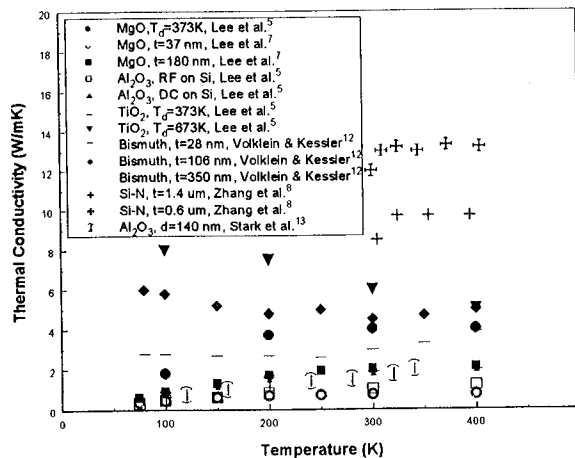
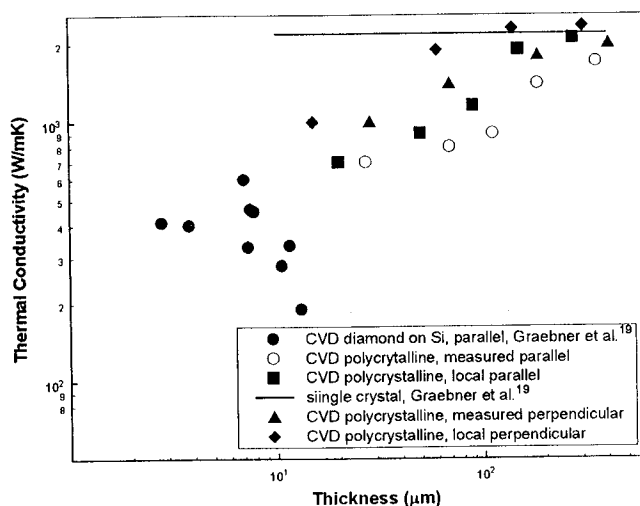


Figure 10. Thermal conductivity of  $\text{SiO}_2$  as a function of film thickness.



**Figure 11.** Thermal conductivity of several different thin film materials as a function of temperature.

that the thermal conductivity of  $\text{TiO}_2$  (Lee et al.<sup>5</sup>) is extremely dependent upon the substrate temperature. The thermal conductivity of  $\text{MgO}$  (Lee et al.<sup>5</sup>) on the other hand is nearly independent of substrate temperature. The thermal conductivity data for aluminum oxide (Lee et al.<sup>5</sup>) show a significant difference between films deposited via dc and rf sputtering techniques. Figure 11 also indicates that, with an increase in temperature, the thermal conductivity of the  $\text{SiO}_2$ - $\text{Si}_3\text{N}_4$  sandwich system increases, whereas, the thermal conductivity of the Si-N (Zhang<sup>8</sup>) appears to be temperature independent.



**Figure 12.** Thermal conductivity of diamond films as a function of thickness.

Figure 12 shows the thermal conductivity of bulk and diamond films as a function of thickness. The thermal conductivity of CVD diamond, in the parallel and perpendicular directions, increases with an increase in thickness and approaches single crystal values. Figure 12 also indicates that the thermal conductivity thin diamond films are lower than thicker polycrystalline films.

### Conclusions

Several different experimental and analytical techniques used to measure the thermal conductivity of thin films have been described. A comparison of the results obtained by these different techniques has also been made. It is apparent that the thermal conductivity of thin film materials is extremely dependent upon several parameters, which include: film thickness, film and substrate temperature, and temperature and method of thin film deposition. Therefore, it is critical that thermal conductivity measurements be made on samples that possess similar microstructures to those used in real devices.

### References

- <sup>1</sup>Okuda, M., Ohkubo, S., "A Novel Method for Measuring the Thermal Conductivity of Submicrometre Thick Dielectric Films," *Thin Solid Films*, Vol. 213, 1992, pp. 176-181.
- <sup>2</sup>Cahill, D.G., Fischer, H.E., Klitsner, T., Swartz, E.T., and Pohl, R.O., "Thermal Conductivity of Thin Films: Measurements and Understanding," *J. Vac. Sci. Technol. A* 7(3), May/June 1989, pp. 1259-1266.
- <sup>3</sup>Cahill, D.G. and Pohl, R.O., "Thermal Conductivity of Amorphous Solids above the Plateau," *Physical Review B*, Vol. 35, 1987, pp. 4067-4073.
- <sup>4</sup>Swartz, E.T. and Pohl, R.O., "Thermal Resistance at Interfaces," *Applied Physics Letters*, Vol. 51, December 197, pp. 2200-2202.
- <sup>5</sup>Lee, S.M. and Cahill, D.G., and Allen, T.H., "Thermal Conductivity of Sputtered Oxide Films," *Physical Review B*, Vol. 52, July 1 1995, pp. 253-257.
- <sup>6</sup>Cahill, D.G., Katiyar, M., and Abelson, J.R., "Thermal Conductivity of  $\alpha$ -Si:H Thin Films," *Physical Review B*, Vol. 50, September 1 1994, pp. 6077-6081.
- <sup>7</sup>Lee, S.M. and Cahill, D.G., "Influence of Interface Thermal Conductance on the Apparent Thermal Conductivity of Thin Films," 2nd US/Japan-Molecular and Microscale Phenomena Conf., August 8-10, 1996, Santa Barbara, CA.
- <sup>8</sup>Zhang, X. and Grigoropoulos, P., "Thermal Conductivity and Diffusivity of Free Standing Silicon Nitride Thin Films," *Rev. Sci. Instrum.*, Vol. 66(2), February 1995, pp. 1115-1120.

- <sup>9</sup>Powell, R.W., *Journal of Scientific Instruments*, Vol. 34., 1957, p. 485.
- <sup>10</sup>Lamropoulos, J.C., Jacobs, S.D., Burns, S.J., Shaw-Klein, L., Hwang, S.S., "Thermal Conductivity of Thin Films: Measurements and Microstructural Effects," HTD-Vol 184, Thin Film Heat Transfer: Properties and Processing, ASME 1991, pp. 21-32.
- <sup>11</sup>Völklein, F., "Thermal conductivity and diffusivity of a thin film  $\text{SiO}_2$  - $\text{Si}_3\text{N}_4$  sandwich system," *Thin Solid Films*, Vol. 188, 1990, pp. 27-33.
- <sup>12</sup>Völklein F. and Kessler E., "Methods for the measurement of thermal conductivity and thermal diffusivity of very thin films and foils," *Measurement*, Vol. 5, 1987, pp. 38-45.
- <sup>13</sup>Stark, I., Stordeur, M., and Syrowatka, F., "Thermal Conductivity of Thin Amorphous Alumina Films," *Thin Solid Films*, Vol. 226, 1993, pp. 185-190.
- <sup>14</sup>Schafft, H.A., Suehle, J.S., and Mirel, P.G.A., "Thermal Conductivity Measurements of Thin Film-Silicon Dioxide," *Proc. IEEE 1989 Int. Conference on Microelectronic Test Structures*, Vol. 2, No. 1, March 1989, pp. 121-125
- <sup>15</sup>Brotzen, F.R., Loos, P.J., and Brady, D.P., "Thermal Conductivity of Thin  $\text{SiO}_2$  Films," *Thin Solid Films*, Vol. 207, 1992, pp.197-201.
- <sup>16</sup>Goodson, K.E., Flik, M.I., Su, L.T., and Antoniadis, D.A., "Annealing Temperature Dependence of the Thermal Conductivity of LPCVD Silicon-Dioxide Layers," *IEEE Electron Device Letters*, Vol. 14, No. 10, October 1993, pp. 490-492.
- <sup>17</sup>Goodson, K.E., Flik, M.I., Su, L.T., and Antoniadis, D.A., "Prediction and Measurement of Thermal Conductivity of Amorphous Dielectric Layer," *Journal of Heat Transfer*, Vol. 116, May 1994, pp. 317-324.
- <sup>18</sup>Kading, O.W., Skurk, H., and Goodson, K.E., "Thermal Conduction normal to Metallized Silicon-Dioxide Layers on Silicon," *Applied Physics Letters*, Vol. 65, 1994, pp. 1629-1631.
- <sup>19</sup>Graebner, J.E., Mucha, J.A., Seibles, L., and Kammlott, G.W., "The Thermal Conductivity of Chemical Vapor Deposited Diamond Films on Silicon," *Journal of Applied Physics*, Vol. 71, 1992b, pp. 3143-3146.
- <sup>20</sup>Graebner, J.E., Jin, S., Kammlott, G.W., Herb, J.A., and Gardinier, C.F., "Unusually High Thermal Conductivity in Diamond Films," *Appl. Phys Lett.*, Vol 60, 1992a, pp. 1576-1578.
- <sup>21</sup>Berman, R., "Thermal Conduction in Solids," Oxford University Press, Oxford, Oxford, 1976.
- <sup>22</sup>Graebner, J.E., Jin, S., Kammlott, G.W., Herb, J.A., and Gardinier, C.F., "Large Inisotropic Thermal Conductivity in Synthetic Diamond Films," *Nature*, Vol. 359, October 1, 1992, pp. 401-403.
- <sup>23</sup>Graebner, J.E., Jin, S., Kammlott, G.W., Bacon, B., Seibles, L., and Banholzer, W., "Anisotropic thermal conductivity in chemical vapor deposited diamond," *Journal of Appl. Physics*, Vol. 71, June 1992, pp. 5353-5356.
- <sup>24</sup>Hetherington, A.V., Wort, C.J.H., and Southwort, P.J., "Crystalline perfection of chemical vapor deposited diamond films," Vol. 5, Aug. 1990, pp. 1591-1594.
- <sup>25</sup>Goodson, K.E., "Thermal Conduction in Nonhomogeneous CVD Diamond Layers in Electronic Microstructures," *Journal of Heat Transfer*, May 1996, Vol. 118, pp. 279-286.
- <sup>26</sup>Ziman, J.M., "Electrons and Phonons," Oxford University Press, Oxford, United Kingdom.
- <sup>27</sup>Anderson, R.J., "The Thermal Conductivity of Rare-Earth-Transition-Metal Films as determined by the Wiedemann-Franz Law," *Journal of Applied Physics* 67(11), June 1 1990, pp. 6914-6916.
- <sup>28</sup>Kittel, C., "Introduction to Solid State Physics," John Wiley & Sons, New York, 1996.
- <sup>29</sup>Redondo, A. and Beery, J.G., "Thermal Conductivity of Optical Coatings," *Journal of Applied Physics*, Vol. 60, December 1996, pp. 3882-3885.
- <sup>30</sup>Swimm, R.T., "Photoacoustic Determination of Thin-Film Properties," *Applied Physics Letters* 42(11), June 1 1983, pp. 955-957.